Applied Catalysis B: Environmental 84 (2008) 533–540

Contents lists available at ScienceDirect

Applied Catalysis B: Environmental

journal homepage: www.elsevier.com/locate/apcatb

Hydrodechlorination of trichloroethene using stabilized Fe-Pd nanoparticles: Reaction mechanism and effects of stabilizers, catalysts and reaction conditions

Feng He, Dongye Zhao *

Environmental Engineering Program, Department of Civil Engineering, 238 Harbert Engineering Center, Auburn University, Auburn, AL 36849, USA

ARTICLE INFO

Article history:
Received 4 July 2007
Received in revised form 4 May 2008
Accepted 13 May 2008
Available online 23 May 2008

Keywords:
Dechlorination
Nanoparticles
Remediation
Stabilizer
Zero-valent iron (ZVI)

ABSTRACT

This study investigated the effects of carboxymethyl cellulose (CMC) as a stabilizer on the reactivity of CMC-stabilized Fe-Pd bimetallic nanoparticles toward trichloroethene (TCE). Overall, the particle stabilization prevented particle agglomeration and resulted in greater particle reactivity. The pseudo-first order TCE degradation rate increased from 0.86 h^{-1} to 6.8 h^{-1} as the CMC-to-Fe molar ratio increased from 0 to 0.0124. However, a higher CMC-to-Fe ratio inhibited the TCE degradation. Within the same homologous series, CMC of greater molecular weight resulted in more reactive nanoparticles for TCE hydrodechlorination. Hydrogen (either residual hydrogen from zero-valent iron (ZVI) nanoparticle synthesis or hydrogen evolved from ZVI corrosion) can serve as effective electron donors for TCE dechlorination in the presence of Pd (either coated on ZVI or as separate nanoparticles). Decreasing reaction pH from 9.0 to 6.0 increased the TCE reduction rate by 11.5 times, but enhanced the Fe corrosion rate by 31.4 times based on the pseudo-first order rate constant. Decreasing pH also shifted the rate controlling step of TCE reduction from Fe corrosion to hydrodechlorination. Ionic strength (<0.51 M) did not significantly affect the TCE reduction.

1. Introduction

Nanoscale zero-valent iron (ZVI) has attracted growing attention in the past decade or so for remediation of groundwater and soils contaminated with chlorinated solvents [1–10], heavy metals [11,12], arsenic [13,14], nitrate [15] and perchlorate [16]. Compared to conventional granular iron particles, ZVI nanoparticles offer the advantage of being more flexibly deliverable into contaminated soils, and thus, can be applied in situ. This advantage can potentially eliminate the need for excavation, and relieve remediation practices from the limitations of depth, site topography, and facility operations. Another potential advantage of ZVI nanoparticles is their high reactivity. The degradation rate of the target contaminants determines the site cleanup time and consequently the remediation cost. It was reported that ZVI nanoparticles can degrade TCE one order of magnitude faster than iron filings [5]. However, because of the very high surface energy, ZVI nanoparticles tend to agglomerate in water rapidly to form micron-scale or larger aggregates, thereby losing their soil mobility and reactivity [1,17–19]. For example, the mass-normalized rate constant for dechlorination of trichloroethene (TCE) by aggregated ZVI nanoparticles was reported only in the order of 10^{-2} L g^{-1} h^{-1} [3,5].

To enhance the reactivity of ZVI nanoparticles toward chlorinated solvents, researchers plated trace amounts of a metal catalyst such as Pd, Ni, and Pt onto the ZVI particles, resulting in various bimetallic nanoparticles [1,5,7–10]. Numerous studies have demonstrated that the iron-based bimetallic particles can degrade chlorinated hydrocarbons such as TCE in water much faster than monometallic ZVI particles [1,5,7–10].

Reduction of chlorinated compounds by bimetallic particles is a hydrodechlorination process, where Fe acts as the electron source, and the metal additive as a catalyst. Consequently, the metal additive's capacity to generate and sorb the reactive atomic hydrogen determines the dechlorination reactivity [5,20–22]. Researchers claimed that the galvanic couples formed between iron and a metal additive are critical for the generation of the reactive atomic hydrogen in the bimetallic systems [5,22]. On the other hand, Cwiertny et al. [20] pointed out that the rate of Fe corrosion is related to the specific properties and loadings of the metal additives. However, it remains unclear how the metal additives affect the TCE reduction with ZVI-Me (Me = a metal catalyst) nanoparticles.

Our recent work [1,2,23] indicated that applying a stabilizer not only prevents aggregation of ZVI nanoparticles, but also results in enhanced overall degradation effectiveness due to the greater

* Corresponding author. Tel.: +1 334 844 6277; fax: +1 334 844 6290.
E-mail address: dzhao@eng.auburn.edu (D. Zhao).

0926-3373/$ – see front matter © 2008 Elsevier B.V. All rights reserved.
doi:10.1016/j.apcatb.2008.05.008

specific surface area of finer nanoparticles. To this end, some water-soluble polysaccharides (e.g. starch and cellulose) have shown themselves to be among the best stabilizers for their low cost and environmental compatibility. Moreover, it was demonstrated that the stabilizers can be used to regulate the iron nucleation and particle growth during the nanoparticle formation and effectively prevent agglomeration of the resultant ZVI nanoparticles [23], thus providing a convenient means for manipulating the size and reactivity of ZVI nanoparticles. Yet, detailed investigation into the effect of particle stabilization on the dechlorination reactivity has been lacking. Moreover, as many other factors such as pH, the type and amount of metal additives have been reported to affect the reactivity of non-stabilized bimetallic ZVI nanoparticles [8,24], effects of these factors on the particle reactivity in the presence of a stabilizer have not been investigated, and our knowledge on the catalytic degradation of TCE is rudimentary.

The overall objective of this study was to investigate the effects of stabilizers, metal additives, pH and ionic strength on the reactivity of CMC-stabilized bimetallic nanoparticles and to acquire further insights into the underlying TCE reduction mechanisms. Sodium carboxymethyl cellulose (CMC) of various molecular weights (M.W.) were tested as model stabilizers. The following key factors were investigated: (1) CMC/Fe^{2+} molar ratio and CMC M.W.; (2) loading and type of a metal catalyst; and (3) reaction pH and ionic strength. Moreover, a conceptual model was proposed to understand the TCE reduction mechanism with the stabilized bimetallic nanoparticles.

2. Materials and methods

2.1. Chemicals

The following chemicals were used as received: $FeSO_4{\cdot}7H_2O$ (Acros Organics, Morris Plains, NJ, USA); sodium carboxymethyl cellulose (CMC): CMC90k (M.W. = 90k, degree of substitution D.S. = 0.7, Acros Organics), CMC250k (M.W. = 250k, D.S. = 0.7, Acros Organics), HP-5A (M.W. = 13k, D.S. = 0.78, Montello, Tulsa, OK, USA); sodium borohydride ($NaBH_4$, ICN Biomedicals, Aurora, OH, USA); $Na_2PdCl_4{\cdot}3H_2O$ (99%, Strem Chemicals, Newburyport, MA, USA); trichloroethylene (TCE) (>99%, spectrophotometric grade, Aldrich, Milwaukee, WI, USA); hexane (pesticide grade, Fisher, Fair Lawn, NJ, USA); nickel chloride (Fisher); copper chloride dihydrate (Acros Organics); $H_2PtCl_6{\cdot}6H_2O$ (99.9%, Acros Organics) and HEPES buffer (Fisher).

2.2. Preparation of nanoparticles

Various stabilized ZVI nanoparticles were prepared by modifying the borohydride-reduction approach using various CMCs as a stabilizer [2,23]. In brief, the preparation was carried out in a 250 mL flask attached to a vacuum line. In a typical preparation, 10 mL freshly prepared stock solution of 0.21 M $FeSO_4{\cdot}7H_2O$ was added to 100 mL of a CMC solution, resulting in a desired concentration of Fe^{2+} and CMC (0–1.0 wt.%). The mixture was then sparged with N_2 for 15 min to assure formation of Fe^{2+}-CMC complex and to remove dissolved oxygen (DO).

ZVI nanoparticles were then obtained by reducing Fe^{2+} ions using 10 mL of a borohydride solution (introduced at 5 mL min^{-1}) at a BH_4^--to-Fe^{2+} molar ratio of 2.0, which was equivalent to the stoichiometric amount. The final ZVI concentration was 0.1 g L^{-1}. To ensure efficient use of BH_4^-, the reactor system was operated under anoxic conditions through continuously vacuuming. The reactor was shaken at 230 rpm until gas (hydrogen) evolution ceased (after ~5 min) and left still for 10 more minutes. Then, the Fe nanoparticles were either tested as monometallic particles or loaded with trace amounts (up to 0.2 wt.% of Fe) of a second metal (Pd, Pt, Ni or Cu) to yield the CMC-stabilized bimetallic nanoparticles. The loading was accomplished by adding known quantities of a metal salt into the CMC-stabilized ZVI nanoparticle suspension [1]. To test the effect of residual H_2 from the nanoparticle preparation, select nanoparticle suspensions were sparged with N_2 for 5 min to remove the residual H_2, and then tested. In all cases, the degradation tests were performed within 5 min after preparation. To test pH effects, TCE degradation tests were also carried out at various pH levels (6.0–9.0) in the presence of 50 mM HEPES buffer.

To probe the role of Pd in TCE degradation with the stabilized Fe-Pd nanoparticles, CMC-stabilized mono-metallic Pd nanoparticles were also synthesized by reducing Pd^{2+} ions with sodium borohydride ($NaBH_4$) in an aqueous solution. In a typical preparation, 1 mL aliquot of a 0.05 M $Na_2PdCl_4{\cdot}3H_2O$ aqueous solution was added to 250 mL of a 0.15 wt.% CMC aqueous solution. Subsequently, 3.5 mL 0.05 M $NaBH_4$ aqueous solution was added to the system under constant stirring to yield the stabilized Pd nanoparticles [25]. The concentration of the resultant Pd nanoparticles was ~0.2 mM (i.e. 21 mg/L). The Pd nanoparticles were characterized or tested within 24 h.

2.3. Physical characterization

TEM micrographs of dried Fe-Pd and Pd nanoparticles were obtained using a Zeiss EM10 Transmission Electron Microscope (Zeiss, Thornwood, NJ, USA). The mean hydrodynamic diameter of the prepared ZVI nanoparticles was determined with a dynamic light scattering (DLS) submicron particle sizer (Nicomp 380, PSS, Santa Barbara, CA, USA). Detailed procedures on TEM and DLS analyses have been described elsewhere [1,2].

2.4. Degradation of TCE

Batch experiments were conducted in 43 mL amber glass vials, filled with 43 mL of a suspension of a certain type of nanoparticles and capped with Teflon septa (the headspace was set to nearly zero to minimize volatilization loss of TCE). TCE degradation was initiated by spiking 25 μL of a TCE stock solution (34.4 g L^{-1} TCE in methanol) into the nanoparticle suspensions, which resulted in an initial TCE concentration of 20 mg L^{-1}. The bottles were then mixed on a rotary shaker (50 rpm) operated at room temperature (~22 °C). At selected times, 0.1 mL of aqueous samples were withdrawn from the reactors using a 100 μL gas-tight syringe. Then the samples were transferred into 2-mL GC vials, each of which containing 1 mL of hexane for extraction of TCE. Upon phase separation, the extracts were analyzed for TCE using a HP 6890 GC equipped with electron capture detector (ECD). All the experimental points were duplicated in two consecutive experiments.

2.5. Analytical methods

TCE was analyzed using an HP 6890 GC equipped with an RTX-624 capillary column (Restek Co, Bellefonte, PA) and an ECD. The detailed procedures have been provided elsewhere [1].

3. Results and discussion

3.1. Effects of CMC stabilizers on hydrodechlorination of TCE by stabilized Fe-Pd nanoparticles and role of H_2

Our previous study [23] showed that the size of CMC-stabilized ZVI nanoparticles can be manipulated by tuning the CMC-to-Fe^{2+}

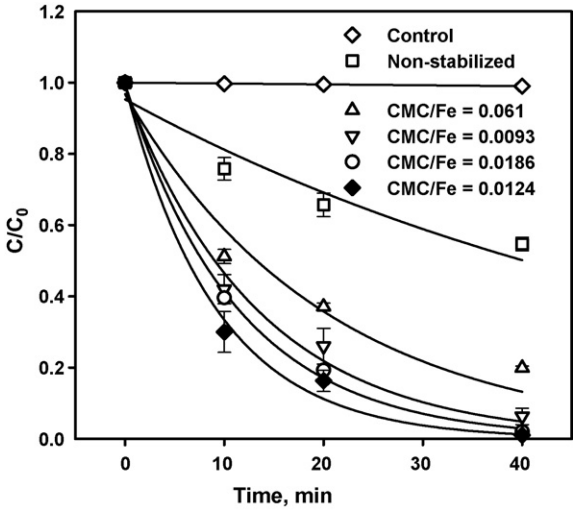

Fig. 1. Hydrodechlorination of TCE using Fe-Pd nanoparticles stabilized with CMC90k at various CMC-to-Fe (CMC/Fe) molar ratios. Initial TCE concentration (C_0) = 20 mg L^{-1}, iron dose = 0.1 g L^{-1} as Fe, Pd:Fe mass ratio = 1.0 mg Pd/g Fe, reaction pH 8.3 ± 0.2. Symbols: mean of experimental duplicates; error bars: range of duplicates; lines: the first-order model fittings.

ratio during the particle synthesis. In general, the higher the CMC-to-Fe^{2+} ratio, the smaller and more monodisperse ZVI nanoparticles were obtained. In this study, the reactivity of CMC-stabilized Fe-Pd nanoparticles (synthesized at various CMC90 k-to-Fe^{2+} molar ratios) was investigated through batch TCE degradation tests. Fig. 1 shows the TCE degradation kinetic data for the Fe-Pd particles stabilized at various CMC-to-Fe^{2+} ratios. The rate data in Fig. 1 are fitted with the following pseudo-first order rate law:

$$-\frac{dC}{dt} = k_{obs}C = k_{SA}a_s\rho_m C \quad (1)$$

where C is the aqueous phase TCE concentration (mg L^{-1}) at time t (min), k_{obs} is the observed pseudo-first order rate constant, k_{SA} is the surface area-based rate constant (L min^{-1} m^{-2}), a_s is the specific surface area of the nanoparticles (m^2 g^{-1}), and ρ_m is the mass concentration of the nanoparticles (g L^{-1}). It is worth noting that the fits of the pseudo-first order kinetics to the experimental data are somewhat poor. The reason for this deviation will be further discussed in later sections.

Fig. 1 shows that the pseudo-first order TCE degradation rate increased from 0.86 h^{-1} to 6.8 h^{-1} as the CMC-to-Fe molar ratio increased from 0 to 0.0124 (i.e. when CMC90k was increased from 0 to 0.2 wt.% for a fixed ZVI concentration of 0.1 g L^{-1}). However, a further increase of the CMC-to-Fe molar ratio from 0.0124 to 0.0186 slightly inhibited the TCE degradation, especially at the beginning of the reactions. Our previous study showed that the size of ZVI nanoparticles was reduced from >200 nm to ~18.6 nm when the CMC-to-Fe molar ratio was increased from 0.0093 to 0.0124 [23]. Therefore, a >11 times faster TCE reduction rate would be expected as the CMC-to-Fe molar ratio increased from 0.0093 to 0.0124 based on the gain in specific surface area (the estimated specific surface area of ZVI particles with diameter of 200 nm and 18.6 nm is 3.8 m^2 g^{-1} and 41.0 m^2 g^{-1}, respectively). However, the TCE reduction rate (k_{obs}) was increased by only a factor of 1.7 (from 4.1 h^{-1} to 6.8 h^{-1}). Apparently, the increase of the dechlorination reactivity in Fig. 1 was not proportional to the gain in the specific surface area of the ZVI nanoparticles. When the CMC-to-Fe molar ratio was further increased from 0.0124 to 0.0186, the ZVI particle size was slightly reduced from 18.6 nm to 17.6 nm [23]. However, the reactivity of the nanoparticles started to decline, and the degradation was further inhibited as the CMC-to-Fe molar ratio was further increased to 0.061 (Fig. 1). Considering that more CMC molecules are adsorbed to the surface of the nanoparticles at higher CMC-to-Fe ratios, this observation suggests that accumulation of CMC molecules on the nanoparticle surface can render a good fraction of the reactive surface unavailable for TCE degradation, and thus, greatly diminish the gained surface area. Evidently, there exists an optimum CMC-to-Fe ratio (~0.0124), where the dechlorination reactivity is maximized and above which the inhibitive effect of CMC overweighed the positive effect from the reduced particle size. In addition to the direct surface occupation, the sorbed CMC molecules can form a more compact surface coating on the particle surface at elevated CMC concentration, which can hinder the mass transfer of TCE to the reactive sites of the Fe-Pd surface. This observation is consistent with several recent published findings [26–29]. For example, Doong and Lai [26] reported that humic acids competed for the reactive sites on the microscale Fe-Pd with tetrachloroethylene (PCE), and thus, lowered the dechlorination rate of PCE. Saleh et al. [27] reported that the reactivity of monometallic ZVI nanoparticles was reduced due to surface coating with surfactants and copolymers.

It should be noted that during the nanoparticle preparation, a relatively large amount of hydrogen gas is formed according to Eqs. (2) and (3) [30,31],

$$Fe(H_2O)_6^{2+} + 2BH_4^- \rightarrow Fe^0 + 7H_2 + 2B(OH)_3 \quad (2)$$

$$2H_2O + BH_4^- \rightarrow BO_2^- + 4H_2 \quad (3)$$

Compared to Eq. (2), Eq. (3) is much slower [30,31]. Eq. (2) indicates that for each mole of Fe^0 formed, seven moles of hydrogen gas is produced. Although the particle preparation was carried out under vacuum, no attempt was made to completely remove the resultant H_2 before the tests in Fig. 1 were conducted. However, because the same particle preparation procedure was followed, the initial amount of H_2 for all cases of Fig. 1 was considered at a comparable level. Our recent study showed that in the presence of CMC-stabilized Pd nanoparticles (2.4 nm, 1 mg L^{-1}), H_2 was able to serve as an effective electron source for rapid and complete degradation of TCE [25]. Therefore, the TCE degradation in Fig. 1 was attributed to reactions with both ZVI nanoparticles and H_2, i.e.

$$C_2HCl_3 + 4Fe^0 + 5H_2O \xrightarrow{Pd} C_2H_6 + 4Fe^{2+} + 3Cl^- + 5OH^- \quad (4)$$

$$C_2HCl_3 + 4H_2 \xrightarrow{Pd} C_2H_6 + 3H^+ + 3Cl^- \quad (5)$$

Consequently, the reaction rate law represented by Eq. (1) is chemically incorrect for fitting the TCE degradation data although it has been commonly used to quantify the overall "lumped" degradation rate. In this particular case, fairly significant discrepancies between the model fittings and experimental data were observed. From an electron balance viewpoint, conversion of Fe^0 to H_2 will not affect the amount TCE degraded. However, caution should be exercised when the residual H_2 from the particle synthesis is present as in Fig. 1. This excess H_2 may lead to overestimation of the reactivity of the stabilized Fe-Pd nanoparticles. For example, Lien and Zhang [32] reported a k_{SA} value of 0.018 L h^{-1} m^{-2} for their nonstabilized Fe-Pd nanoparticles (after drying), whereas, a k_{SA} value of 0.24 L h^{-1} m^{-2} for nonstabilized Fe-Pd nanoparticles prepared in this study can be obtained if same surface area was assumed (e.g. 35 m^2/g). The reported unusually high rate constants for starch-stabilized [1] and CMC-stabilized Fe-Pd nanoparticles [2] may also be partially attributed to the residual H_2. On the other hand, discarding the H_2 from the particle synthesis (as commonly is the case) represents a tremendous waste of electron source which is equally effective as Fe^0 for TCE degradation, but offers 8 times more electrons (Eq. (2)).

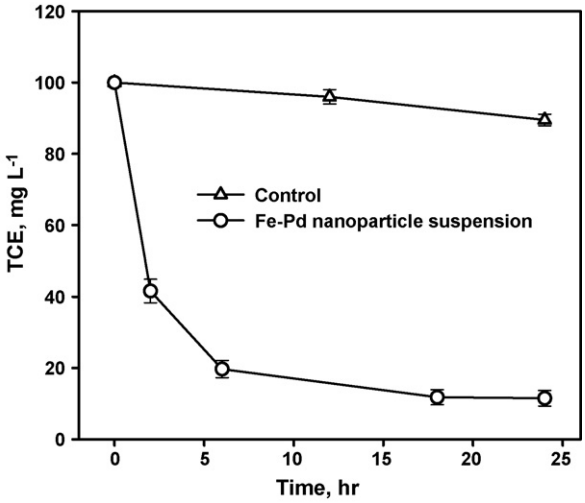

Fig. 2. Degradation of TCE by CMC-stabilized Fe-Pd nanoparticles and by residual hydrogen from the nanoparticle synthesis. Iron dose = 0.1 g L^{-1} Fe^0, C_0 = 100 mg L^{-1} TCE, CMC90k = 0.2 wt.%, Pd:Fe mass ratio = 1.0 mg Pd/g Fe. Data given as mean of experimental duplicates with the range.

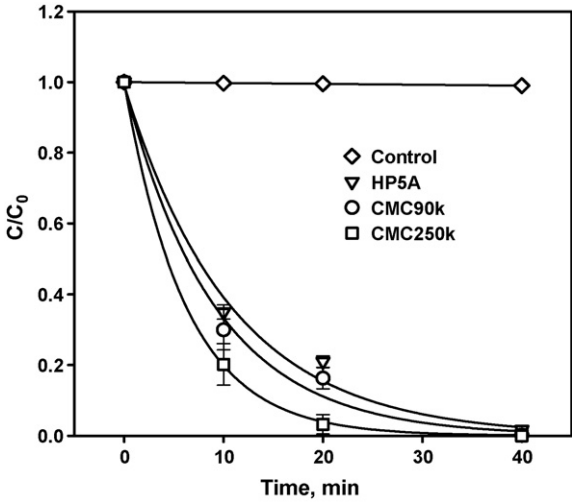

Fig. 3. Hydrodechlorination of TCE using Fe-Pd nanoparticles stabilized with CMCs of various M.W. Iron dose = 0.1 g L^{-1} Fe, C_0 = 20 mg L^{-1} TCE, CMC = 0.2 wt.% for all cases, Pd:Fe mass ratio = 1.0 mg Pd/g Fe, reaction pH 8.3 ± 0.2. *Symbols*: mean of experimental duplicates; *error bars*: range of duplicates; *lines*: the first-order model fittings.

To demonstrate and estimate the magnitude of the added reducing power from the residual hydrogen, TCE degradation tests were carried out at an initial TCE concentration of 100 mg L^{-1} and a ZVI nanoparticle dose of 0.1 g L^{-1}. Based on the reaction stoichiometry, the electrons from the ZVI nanoparticle dose can only transform a maximum of 53.0 mg L^{-1} TCE, i.e. TCE was nearly 2 times in excess of the ZVI nanoparticles. However, Fig. 2 shows that 88.5 ± 2.2% of the TCE was degraded at equilibrium (after ~1 day). Considering a TCE loss of 10 mg L^{-1} based on the control tests, an extra 25 mg L^{-1} TCE was degraded in the system. Therefore, the residual H_2 from the ZVI nanoparticle preparation (Eq. (2)) was acting as additional electron donors.

The size of Fe nanoparticles can also be altered by using CMCs of various M.W. or of different functionalities as a stabilizer [23]. At a fixed CMC-to-Fe^{2+} molar ratio of 0.0124, the application of three CMC stabilizers HP5A (M.W. = 13k), CMC90k (M.W. = 90k), and CMC250k (M.W. = 250k) resulted in Fe nanoparticles (0.1 g L^{-1}) of >200 nm, 18.6 nm, and 15.6 nm, respectively [23]. Fig. 3 shows that the smaller nanoparticles (stabilized with CMC of greater M.W.) exhibited greater reactivity for TCE degradation. The three CMC stabilizers bear homologous chain-like molecular structures with markedly different molecular size (length) but the same repeating units. Our prior FT-IR [2] studies indicated that the CMC molecules are adsorbed on the ZVI nanoparticle surface via the $-COO^-$ and –OH groups. From the standpoint of both the stereochemistry of the CMC molecules and thermodynamic stability of the system, it is plausible that only a fraction of the $-COO^-$ and –OH groups in the CMC molecules are involved in interacting with the ZVI particles. Therefore, the larger the CMC molecules, the fewer molecules are adsorbed to the nanoparticles, thus leaving more sites available for reactions [25].

3.2. Effects of Pd coated on ZVI and Pd added as separate nanoparticles

Numerous studies have demonstrated the formation of Fe-Pd bimetallic particles with adding Pd^{2+} to microscale ZVI [26,33]. In this study, it is expected that Fe-Pd bimetallic nanoparticles were formed upon the addition of Pd^{2+} ions to Fe nanoparticle suspension. To gain a deeper insight into the role of Pd in TCE degradation by stabilized Fe-Pd nanoparticles, monometallic Pd and Fe nanoparticles were first synthesized separately and then mixed and tested for TCE degradation. Fig. 4 shows a typical transmission electron microscopy (TEM) image of the CMC-stabilized monometallic Pd nanoparticles. Based on the TEM image, the mean particle diameter was determined to be 2.4 ± 0.5 nm (S.D.). Fig. 5 compares the TCE degradation rates of the separate Fe and Pd nanoparticles versus Fe-Pd bimetallic nanoparticles under otherwise identical conditions (i.e. Fe = 0.1 g/L and Pd = 0.1 mg/L).

To eliminate the interference of the residual H_2 from the particle preparation, the nanoparticle suspensions were vigorously purged with N_2 for 5 min to remove the H_2 before TCE degradation was initiated. The removal of H_2 was confirmed through GC analysis following the method by Liu et al. [34]. UV–vis measurement of the nanoparticle suspensions before and after N_2 purging showed only ~5% decrease of the absorbance (A) at a wavelength 600 nm, which indicated that the amount of Fe^0 corroded during the N_2 purging was negligible. The UV–vis absorbance was found to be a convenient measure for representing the concentration of suspended ZVI nanoparticles in water [18].

Fig. 4. Representative TEM image of CMC90k-capped Pd nanoparticles. The scale bar represents 30 nm. The average size of 452 particles in this image was determined to be 2.4 ± 0.5 nm (S.D.) using Image J software.

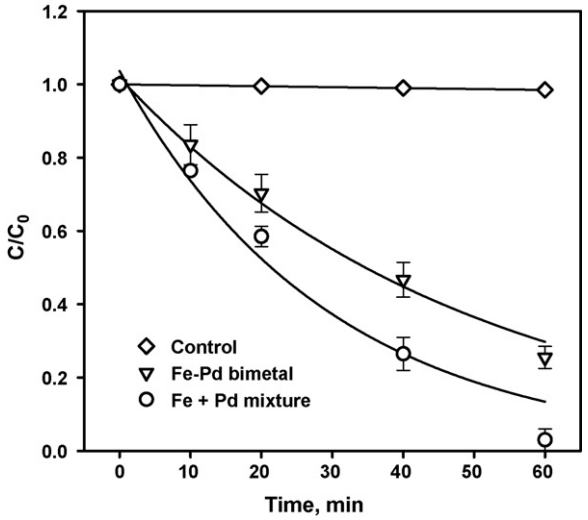

Fig. 5. Hydrodechlorination of TCE using mixture of separately prepared monometallic Pd and Fe nanoparticles as opposed to Fe-Pd bimetallic nanoparticles. Residual H_2 from particle synthesis was removed for all cases. Iron dose = 0.1 g L^{-1} Fe, C_0 = 20 mg L^{-1} TCE, CMC90k = 0.2 wt.%, Pd:Fe mass ratio = 1.0 mg Pd/g Fe, reaction pH 8.3 ± 0.2. *Symbols*: mean of experimental duplicates; *error bars*: range of duplicates; *lines*: the first-order model fittings.

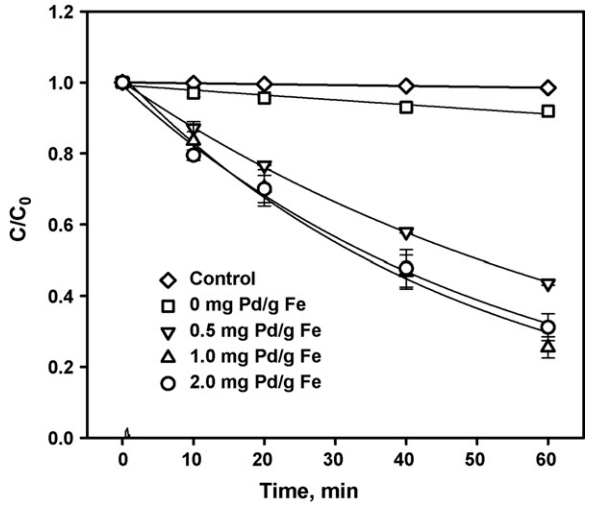

Fig. 6. Effect of Pd loading on hydrodechlorination of TCE by CMC-stabilized Fe-Pd nanoparticles. Residual H_2 from particle synthesis was removed in all cases. Iron dose = 0.1 g L^{-1} Fe, C_0 = 20 mg L^{-1} TCE, CMC90k = 0.2 wt.%, reaction pH 8.3 ± 0.2. *Symbols*: mean of experimental duplicates; *error bars*: range of duplicates; *lines*: the first-order model fittings.

Fig. 5 shows that the mixture of CMC-stabilized monometallic Fe and Pd nanoparticles exhibited a nearly two times greater reactivity toward TCE (k_{obs} = 2.0 h^{-1}) than the Fe-Pd bimetallic nanoparticles (k_{obs} = 1.1 h^{-1}). In the former case, the Pd and Fe nanoparticles are separated by the solution, and thus, there exists a huge activation barrier for Pd to directly catalyze the degradation of TCE by the ZVI nanoparticles. However, the highly reactive ZVI nanoparticles can undergo rapid corrosion reaction with water to give off H_2. Therefore, the observed highly effective degradation of TCE is attributed to reduction by H_2 with the Pd nanoparticles as catalysts. For the bimetallic Fe-Pd nanoparticles, the presence of Pd on the Fe surface is expected to catalyze TCE reduction by both Fe^0 and H_2. However, the slower overall TCE degradation rate with the bimetallic nanoparticles indicates that the overall TCE degradation rate is not limited by the Fe corrosion, but rather by the catalytic activity of Pd. When the results in Fig. 1 and Fig. 5 are compared, it is evident that the removal of the residual H_2 from the particle synthesis reduced the TCE degradation rate (k_{obs}) from 6.8 h^{-1} to 1.1 h^{-1} for the Fe-Pd bimetallic nanoparticles. Based on the data for the Fe-Pd bimetallic nanoparticles in Fig. 5 and a mean TEM-based diameter of 4.3 nm (specific surface area: 177 m^2 g^{-1}) [2], the surface area normalized k_{SA} value was calculated to be 0.0064 L h^{-1} m^{-2}.

3.3. Effect of Pd loading on TCE hydrodechlorination

As has been widely observed, the presence of trace amounts of Pd can substantially catalyze the hydrodechlorination rate. On the other hand, from both economic and environmental standpoints, the amount of Pd applied should be minimized. To this end, a mechanistic and quantitative analysis of the role of Pd is of critical importance. Fig. 6 shows the TCE degradation rates by Fe-Pd bimetallic nanoparticles at various loading of Pd but under otherwise identical conditions. In agreement with our previous study [1], the presence of trace amounts of Pd resulted in much more effective degradation of TCE. At a Pd loading of 0.5 mg Pd/g Fe, a k_{obs} value of 0.84 h^{-1} was obtained, which was one order of magnitude greater than that when only ZVI was used. Further increasing the Pd loading to 1.0 mg Pd/g Fe increased the TCE reduction rate constant to 1.1 h^{-1}. However, when the loading was further increased to 2.0 mg Pd/g Fe, the degradation rate remained nearly unchanged. Kim and Carraway [35] studied the reactivity of micrometer-scale Fe-Pd bimetallic particles for TCE degradation as a function of Pd loading. They observed that the k_{SA} value increased linearly over the range of Pd loadings <0.1 wt.% of Fe (i.e. 1.0 mg Pd/g Fe). However, the increase in k_{SA} became much less considerable when the Pd loading was increased from 0.1 to 0.77 wt.% of Fe. Wei et al. [8] also observed the increase of k_{obs} for 2, 4-chlorophenol reduction over the investigated range of Pd loadings (<1.0 mg Pd/g Fe) with non-stabilized Fe-Pd particles.

When trace amounts of Pd^{2+} ions are added to the ZVI nanoparticle suspension, the cations are reduced by the nanoparticles and end up being plated on the iron surface uniformly to form a monolayer of Pd atoms [36]. The theoretical monolayer surface coverage can be estimated by assuming that the Pd overlayer is predominantly in the lowest energy fcc(1 1 1) crystallographic orientation [36]. Under these conditions, the surface area of one unit cell is given by [36]

$$\text{Surface area per unit cell}\,(\text{nm}^2) = 2 \cdot \sqrt{3} \cdot r^2 \quad (6)$$

where r is the radius of a Pd atom (0.138 nm) [37]. Based on the specific surface area of the iron calculated based on the mean TEM diameter (4.3 nm, 177 m^2 g^{-1}) [2], a full monolayer of Pd atoms would be equivalent to 0.47 g Pd/g Fe.

Therefore, at a Pd loading of <2.0 mg Pd /g Fe, only a small fraction (<0.43%) of the ZVI surface is covered by the Pd atoms. Conceptually, doubling the Pd loading (e.g. from 1.0 to 2.0 mg Pd/g Fe) will double the number of Fe-Pd galvanic cells, which would generate more atomic hydrogen (the reactive species for TCE degradation), and thus, should speed up the TCE reduction rate. However, the fact that little enhancement in the reaction rate was observed as the Pd loading was increased from 1.0 to 2.0 mg Pd/g Fe indicates that the generation of the reactive atomic hydrogen is not controlled by the Fe-Pd galvanic couples, but rather by the corrosion rate of the bulk ZVI surface. It is also evident from Fig. 6 that at a Pd-to-Fe ratio of <1.0 mg Pd/g Fe, the amount of catalyst (Pd) is limiting the degradation rate, whereas the iron corrosion (or formation of atomic hydrogen) becomes the rate-limiting factor when the loading exceeds 1.0 mg Pd/g Fe.

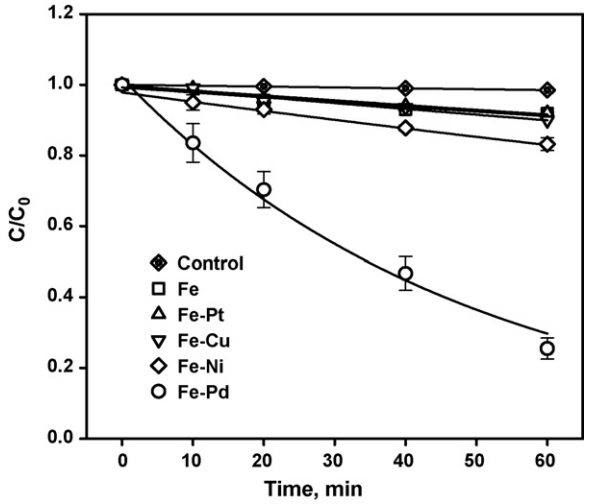

Fig. 7. Effect of various metal catalysts on hydrodechlorination of TCE by CMC-stabilized bimetallic nanoparticles. Residual H_2 from particle synthesis was removed in call cases. Iron dose = 0.1 g L^{-1} Fe, C_0 = 20 mg L^{-1} TCE, CMC90k = 0.2 wt.%, metal:Fe molar ratio = 9.7 μmol metal/g Fe, reaction pH 8.3 ± 0.2. *Symbols*: mean of experimental duplicates; *error bars*: range of duplicates; *lines*: the first-order model fittings.

3.4. Effect of various types of metal catalysts

In addition to Pd, other transition metals such as Ni, Pt and Cu were studied for their catalytic activity toward TCE degradation with the stabilized ZVI nanoparticles. CMC-stabilized bimetallic Fe-Me (where Me = Ni, Pt or Cu) nanoparticles were prepared following the same procedure as for the stabilized Fe-Pd nanoparticles. For all cases, the Me-to-Fe ratio was fixed at 9.7 μmol Me/g Fe, which is equivalent to 1.0 mg Pd/g Fe for the Fe-Pd nanoparticles and 0.57 mg Ni/g Fe, 1.9 mg Pt/g Fe, and 0.62 mg Cu/g Fe for the Fe-Ni, Fe-Pt, and Fe-Cu nanoparticles, respectively. Fig. 7 shows that the catalytic activity of Pd far exceeds that of the other metals. Fig. 7 reveals the following sequence of dechlorination reactivity for the Me-Fe bimetallic nanoparticles: Fe-Pd ≫ Fe-Ni > Fe-Pt ≈ Fe-Cu ≈ Fe, which generally agrees with the results for non-stabilized ZVI particles reported by others [21,22,24,35].

3.5. Mechanisms of TCE degradation by stabilized Fe-Pd nanoparticles

Based on findings in this work and extensive studies on TCE degradation by Fe-Pd bimetal in the open literature (5, 20, 22, 32), the underlying mechanisms of TCE dechlorination by CMC-stabilized Fe-Pd nanoparticles are discussed. In a system containing TCE and the aqueous suspension of CMC-stabilized Fe-Pd nanoparticles, the following reactions can take place:

$$Fe^0 + 2H_2O \rightarrow Fe^{2+} + H_2 + 2OH^- \quad (7)$$

$$Fe^0 + 2H_2O \xrightarrow{Pd} Fe^{2+} + H_2\uparrow + 2OH^- \quad \text{(side reaction)} \quad (8)$$

$$H_2 \xrightarrow{Pd} H^\bullet + {}^\bullet H \quad (9)$$

$$TCE + 8H^\bullet \rightarrow \text{ethane} + 3H^+ + 3Cl^- \quad (10)$$

Liu et al. [3,38] investigated dechlorination of TCE by non-stabilized ZVI nanoparticles, and they asserted that the ZVI particles underwent an oxidative dissolution process with Fe^0 in the particles being fully accessible during TCE reduction. They also observed that a portion of the oxidized iron was transformed to crystalline magnetite in solution. For the CMC-stabilized Fe-Pd nanoparticles, Fe^0 may undergo the same oxidative corrosion (reaction with water) (Eq. (7)) with the resultant Fe^{2+} released into the solution. However, because of the much smaller size, the reactive lifetime for the CMC-stabilized nanoparticles is expected to be shorter than for the non-stabilized counterparts. In addition, CMC can complex with Fe ions, and prevents the resulting iron oxides or iron hydroxides from aggregating and settling as is the case for non-stabilized iron particles. We observed that under ambient conditions, the stabilized Fe-Pd (0.1 g L^{-1}) nanoparticles were completely oxidized in water after ∼7 days without precipitates being observed.

The role of the galvanic corrosion (Eq. (8)) appears insignificant as discussed earlier because of the minimal amounts of Pd loaded (<2.0 mg Pd/g Fe). The galvanic corrosion can be more profound when the surface loading of the metal is high. For example, Schrick et al. [5] observed that the galvanic corrosion rate of non-stabilized bimetallic Fe-Ni (Fe:Ni = 3:1, w/w) particles was much faster than the mixture of monometallic Fe or Ni particles. Lin et al. [22] reported that the corrosion of an Fe powder was promoted as 0.25 wt.% of a noble metal such as Pd, Pt, Au and Ru was plated on the Fe surface. Note that for the Fe powder, this metal loading was enough to form two full atomic layers on the Fe surface because of the much larger particle size of the Fe powder. For comparison, 0.25 wt.% Pd would only cover ∼0.54% of the Fe surface for the CMC-stabilized nanoparticles.

As iron corrodes, protons from water are reduced to atomic H and then to molecular hydrogen at the iron surface (Eq. (7)). The hydrogen is then transferred and sorbed to the palladium lattice where it partially dissociates back to atomic hydrogen (Eq. (9)), which is the primary reactive species for hydrodechlorination. Note that the residual H_2 from ZVI nanoparticle synthesis process can also undergo the same process and degrade TCE. As TCE is transferred onto the surface of Pd atoms, the cleavage of the C–Cl bonds takes place via hydrodechlorination (Eq. (10)). Fig. 8 depicts the degradation mechanism of TCE in the stabilized Fe-Pd bimetallic systems. Ethane is considered to be the final TCE hydrodechlorination product based on the results from prior studies [1,2,32].

Researchers have attributed the different catalytic activity of various metal catalysts to different 'solubility' of atomic hydrogen in each metal additive [20,22], although competing theories exist on what represents a metric for hydrogen solubility. Lin et al. [22] proposed that exchange current densities for hydrogen evolution represent a metric for the hydrogen solubility in metal additives. On the other hand, Cwiertny et al. [20] postulated that the relative partial molar enthalpy for an infinitely dilute solution of atomic hydrogen in each additive is a better metric for atomic hydrogen solubility. Despite the different metrics, both theories support the notion that palladium offers the greatest hydrogen solubility of the tested metals in this study. As expected, palladium was the most efficient metal catalyst for TCE dechlorination in stabilized Fe-Me nanoparticle systems.

3.6. Effect of pH

To investigate pH effects on dechlorination reactivity of the stabilized Fe-Pd nanoparticles, Fe-Pd nanoparticle suspensions at pH ranging from 6 to 9 were prepared by using 50 mM HEPES as a buffer. Fig. 9(a) shows that at a given pH, the degradation of TCE followed pseudo first-order kinetics. The results also indicate a general trend of decreasing reaction rate with increasing pH. This observation is consistent with the results observed for 2,4-dichlorophenol hydrodechlorination by non-stabilized Fe-Pd nanoparticles [8] and reductive dechlorination of TCE and TCA by non-stabilized ZVI nanoparticles [6,38].

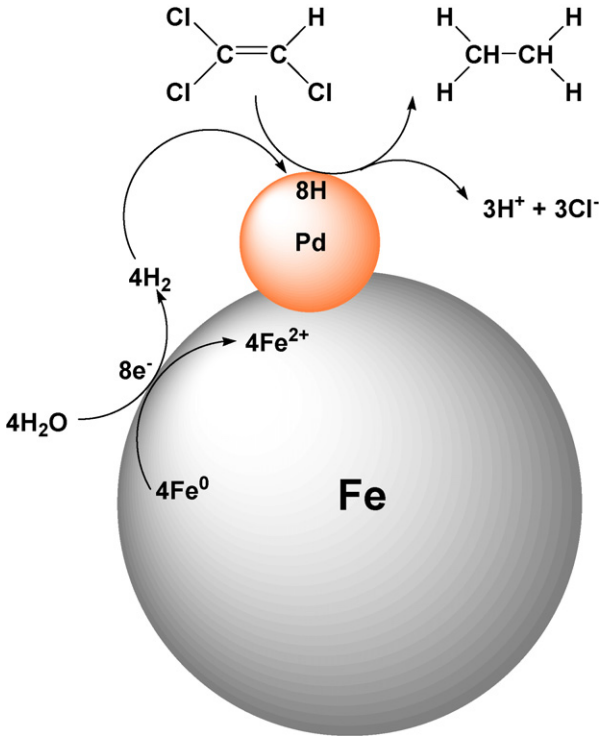

Fig. 8. Illustrative diagram of TCE hydrodechlorination on the surface of CMC-stabilized Fe-Pd nanoparticles.

In accord with the TCE degradation mechanism discussed above, two reactions can limit the TCE degradation rate in stabilized Fe-Pd nanoparticle system. One is the corrosion of ZVI to produce H_2, which is more favored at lower solution pH; and the other is the hydrodechlorination of TCE by H_2 (or atomic hydrogen) at the Pd surface, which is also favored at lower pH since lowering pH produces more H_2. To gain an insight into the relative corrosion rate, the corrosion rate of the CMC-stabilized Fe-Pd nanoparticles in water (no TCE) was monitored by monitoring the transient change in the UV–vis absorbance (A) of the nanoparticle suspensions at a wavelength 600 nm [18], as shown in Fig. 9(b). The Fe corrosion at a given pH also followed the first-order kinetics, and thus, k_{obs} can be determined for each pH. Fig. 9(c) compares the pseudo first-order corrosion rate constants and the TCE degradation constants at each pH. Note that in Fig. 9(c) the rate constants are normalized to the respective rate constant at pH 9.0. Fig. 9(c) also revealed that there exists a strong correlation between iron corrosion and TCE degradation. As pH was lowered from 9.0 to 8.2, both TCE degradation and Fe corrosion rates were increased by ~60%. This observation indicates that at higher pH (e.g. pH > 8.2), Fe corrosion controls the reduction of TCE as a relatively slow process. However, as pH was further decreased from 8.2 to 6.0, the increase in iron corrosion rate far overweighed the TCE reduction rate. For example, from pH 8.2 to 6.0, Fe corrosion rate was increased by ~31.4 times, compared to only 11.5 times for TCE reduction rate. As pH decreases, proton supplies become more abundant, and the rate controlling step gradually shifts from iron corrosion to the hydrodechlorination process, which is governed by the activity and concentration of the catalyst (Pd).

3.7. Effect of ionic strength on TCE dechlorination by stabilized Fe-Pd nanoparticles

To test the effect of ionic strength on TCE degradation by the CMC-stabilized Fe-Pd nanoparticles, sodium chloride at 1.0 wt.% (ionic strength = 0.17 M) and 3.0 wt.% (ionic strength = 0.51 M), respectively, was added into the nanoparticle suspension to simulate conditions of a saline water. Fig. 10 shows that the presence of 1.0 wt.% and 3.0 wt.% NaCl only slightly reduced the

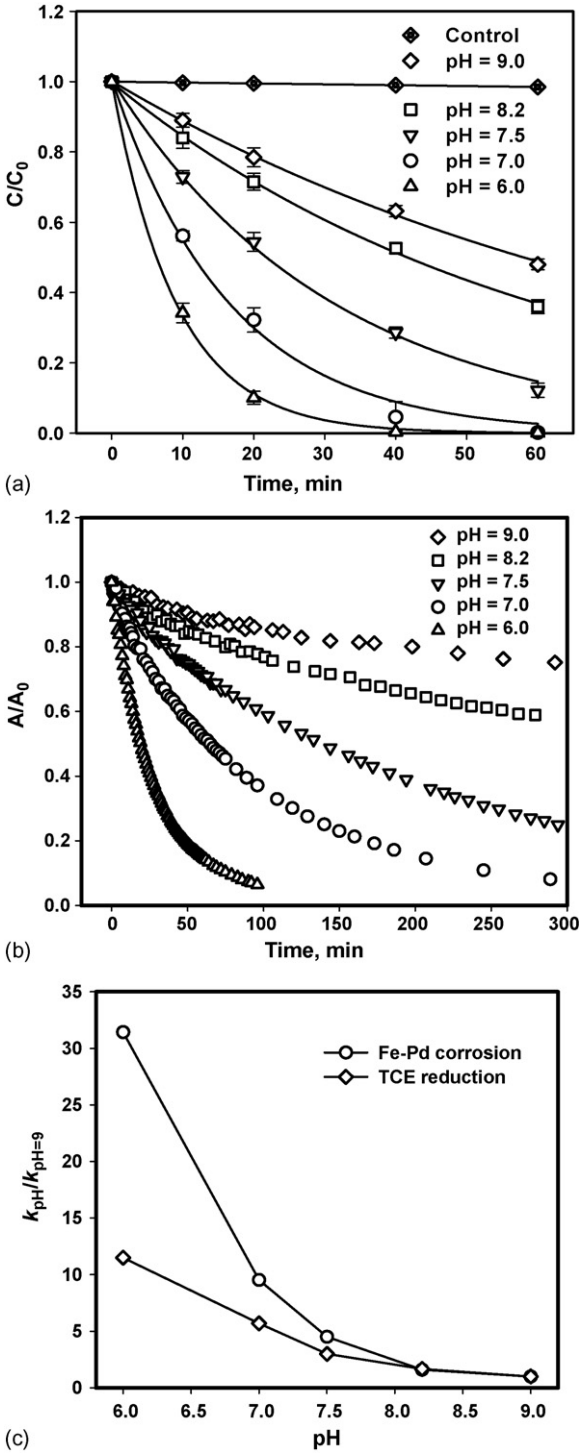

Fig. 9. (a) Hydrodechlorination of TCE by CMC-stabilized Fe-Pd nanoparticles at various pH levels in a 50 mM HEPES buffer with removal of residual H_2 from particle synthesis; (b) corrosion of Fe represented by the decrease of suspension UV–vis absorbance at a wavelength of 600 nm; (c) normalized TCE reaction rate vs. Fe corrosion rate. In call cases, iron dose = 0.1 g L^{-1} Fe, C_0 = 20 mg L^{-1} TCE, CMC90k = 0.2 wt.%, Pd:Fe mass ratio = 1.0 mg Pd/g Fe. *Symbols*: mean of experimental duplicates; *error bars*: range of duplicates; *lines* in (a): the first-order model fittings.

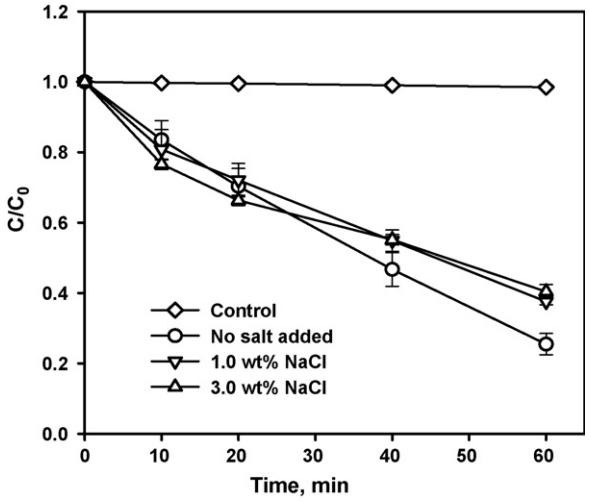

Fig. 10. Hydrodechlorination of TCE by CMC-stabilized Fe-Pd nanoparticles in the presence of high concentration NaCl. Residual H_2 from particle synthesis was removed in all cases. Iron dose = 0.1 g L^{-1} Fe, C_0 = 20 mg L^{-1} TCE, CMC90k = 0.2 wt.%, Pd:Fe mass ratio = 1.0 mg Pd/g Fe, reaction pH 8.3 ± 0.2. Data given as mean of experimental duplicates with the range.

TCE degradation. For example, at the end of the 1-hour test period, the amount of TCE degraded was 62% and 60% with 1.0 and 3.0 wt.% NaCl, compared to 75% when no NaCl was present. Our prior study showed that the presence of high concentrations of Na^+ can cause partial aggregation of the nanoparticles due to the double layer compression effect on the ZVI nanoparticle surface [23]. For instance, the presence of 100 mM (or 0.6 wt.%) NaCl increased the particle size from 18.6 to 33.7 nm. Because of the increased particle size (or reduced specific surface area), the TCE degradation reactivity by the stabilized nanoparticles was slightly reduced. Nevertheless, Fig. 10 indicates that the stabilized Fe-Pd nanoparticles remain highly effective for TCE dechlorination even under highly saline conditions.

4. Conclusions

In this study, effects of particle stabilization, metal catalysts, reaction pH and ionic strength on TCE degradation by CMC-stabilized Fe-Pd nanoparticles were investigated. The key findings from this study are summarized as follows:The concentration, molecular weight and type of stabilizers can affect surface capping chemistry of the Fe-Pd nanoparticles, and thus, the TCE mass transfer behavior on Fe-Pd surface and the TCE reduction rate. Generally, particle stabilization prevented particle agglomeration and resulted in greater particle reactivity. However, CMCs at high concentrations (e.g. CMC-to-Fe molar ratio >0.0124 for CMC90k) may inhibit the reactivity of the nanoparticles. On an equalivalent mass basis, application of CMCs of lower M.W. resulted in slower TCE reduction.H_2 can serve as an effective electron source for TCE degradation in the presence of a metal catalyst such as Pd. In a closed system, the conversion of the electron sources from ZVI to H_2 during the ZVI corrosion does not diminish the TCE reducing power of the nanoparticles.Water reduction on the Fe surface instead of galvanic corrosion was the predominant mechanism for the generation of molecular hydrogen with the stabilized Fe-Pd nanoparticles at a Pd loading less than 2.0 mg Pd/g Fe. At a Pd-to-Fe mass ratio lower than 1.0 mg Pd/g Fe, the amount of catalyst (Pd) limited the degradation rate, whereas the iron corrosion became the rate-limiting factor when the loading exceeded 1.0 mg Pd/g Fe.Decreasing solution pH benefited the TCE reduction in Fe-Pd system but enhanced the corrosion rate to an even greater extent at a Pd loading of 1.0 mg Pd/g Fe. As pH was lowered from 9.0 to 6.0, the rate controlling step of TCE reduction shifted from Fe corrosion to hydrodechlorination.The stabilized bimetallic nanoparticles can highly effectively degrade TCE in both fresh and saline water.

Acknowledgments

We are grateful to Dr. Juncheng Liu for his assistance with TEM analyses. This work was partially supported by a USEPA STAR grant (GR832373).

References

[1] F. He, D. Zhao, Environ. Sci. Technol. 39 (2005) 3314–3320.
[2] F. He, D. Zhao, J. Liu, C.B. Roberts, Ind. Eng. Chem. Res. 46 (2007) 29–34.
[3] Y. Liu, S.A. Majetich, R.D. Tilton, D.S. Sholl, G.V. Lowry, Environ. Sci. Technol. 39 (2005) 1338–1345.
[4] J.T. Nurmi, P.G. Tratnyek, V. Sarathy, D.R. Baer, J.E. Amonette, K. Pecher, C.M. Wang, J.C. Linehan, D.W. Matson, R.L. Penn, M.D. Driessen, Environ. Sci. Technol. 39 (2005) 1221–1230.
[5] B. Schrick, J.L. Blough, A.D. Jones, T.E. Mallouk, Chem. Mater. 14 (2002) 5140–5147.
[6] H. Song, E.R. Carraway, Environ. Sci. Technol. 39 (2005) 6237–6245.
[7] C.B. Wang, W.X. Zhang, Environ. Sci. Technol. 31 (1997) 2154–2156.
[8] J. Wei, X. Xu, Y. Liu, D. Wang, Water Res. 40 (2006) 348–354.
[9] L. Wu, S.M.C. Ritchie, Chemosphere 63 (2006) 285–292.
[10] J. Xu, D. Bhattacharyya, Ind. Eng. Chem. Res. 46 (2007) 2348–2359.
[11] S.M. Ponder, J.G. Darab, T.E. Mallouk, Environ. Sci. Technol. 34 (2000) 2564–2569.
[12] Y. Xu, D. Zhao, Water Res. 41 (2007) 2101–2108.
[13] S.R. Kanel, J.M. Greneche, H. Choi, Environ. Sci. Technol. 40 (2006) 2045–2050.
[14] S.R. Kanel, B. Manning, L. Charlet, H. Choi, Environ. Sci. Technol. 39 (2005) 1291–1298.
[15] Y.H. Liou, S.L. Lo, W.H. Kuan, C.J. Lin, S.C. Weng, Water Res. 40 (2006) 2485–2492.
[16] Z. Xiong, D. Zhao, G. Pan, Water Res. 41 (2007) 3497–3505.
[17] X.Q. Li, D.W. Elliott, W.X. Zhang, Crit. Rev. Solid State Mater. Sci. 31 (2006) 111–122.
[18] N. Saleh, T. Phenrat, K. Sirk, B. Dufour, J. Ok, T. Sarbu, K. Matyiaszewski, R.D. Tilton, G.V. Lowry, Nano Lett. 5 (2005) 2489–2494.
[19] B. Schrick, B.W. Hydutsky, A.D. Jones, T.E. Mallouk, Chem. Mater. 16 (2004) 2187–2193.
[20] D.M. Cwiertny, S.J. Bransfield, K.J.T. Livi, D.H. Fairbrother, A.L. Roberts, Environ. Sci. Technol. 40 (2006) 6837–6843.
[21] Y.H. Kim, E.R. Carraway, Environ. Technol. 24 (2003) 69–75.
[22] C.J. Lin, S.L. Lo, Y.H. Liou, J. Hazard. Mater. 116 (2004) 219–228.
[23] F. He, D. Zhao, Environ. Sci. Technol. 41 (2007) 6216–6221.
[24] W.X. Zhang, C.B. Wang, H.L. Lien, Catal. Today 40 (1998) 387–395.
[25] J. Liu, F. He, J.E. Durham, D. Zhao, C.B. Roberts, Langmuir 24 (2008) 328–336.
[26] R.A. Doong, Y.J. Lai, Water Res. 39 (2005) 2309–2318.
[27] N. Saleh, K. Sirk, Y.Q. Liu, T. Phenrat, B. Dufour, K. Matyjaszewski, R.D. Tilton, G.V. Lowry, Environ. Eng. Sci. 24 (2007) 45–57.
[28] P.G. Tratnyek, M.M. Scherer, B. Deng, S. Hu, Water Res. 35 (2001) 4435–4443.
[29] A.B. Giasuddin, S.R. Kanel, H. Choi, Environ. Sci. Technol. 41 (2007) 2022–2027.
[30] H.I. Schlesinger, H.C. Brown, A.E. Finholt, J.R. Gilbreath, H.R. Hoekstra, E.K. Hyde, J. Am. Chem. Soc. 75 (1953) 215–219.
[31] G.N. Glavee, K.J. Kladunde, C.M. Sorensen, G.C. Hadjipanayis, Inorg. Chem. 34 (1995) 28–35.
[32] H.L. Lien, W.X. Zhang, Colloids Surf. A 191 (2001) 97–105.
[33] G.N. Jovanovic, P. Znidarsic-Plazl, P. Sakrittichai, K. Al-Khaldi, Ind. Eng. Chem. Res. 44 (2005) 5099–5106.
[34] Y. Liu, H. Choi, D. Dionysiou, G.V. Lowry, Chem. Mater. 17 (2005) 5315–5322.
[35] Y.H. Kim, E.R. Carraway, Environ. Technol. 24 (2003) 809–819.
[36] S.J. Bransfield, D.M. Cwiertny, A.L. Roberts, D.H. Fairbrother, Environ. Sci. Technol. 40 (2006) 1485–1490.
[37] R.J.D. Tilley, Understanding Solids: The Science of Materials, John Wiley & Sons, New York, 2004.
[38] Y. Liu, G.V. Lowry, Environ. Sci. Technol. 40 (2006) 6085–6090.